Electrical and Thermal Analysis of an OLED Module

Jurica Kundrata*[1] and Adrijan Baric[1]
[1] Faculty of Electrical Engineering and Computing, University of Zagreb, Croatia
*Corresponding author: Unska 3, 10000 Zagreb, Croatia, jurica.kundrata@fer.hr

Abstract: This paper presents the electrical and thermal analysis of an OLED module. The OLED module consists of the OLED element and the DC-DC converter incorporated in its backplane. The DC-DC converter is realized as an integrated circuit and uses an external inductor. The inductor is embedded in the substrate of the backplane and has a spiral geometry. The DC-DC converter is highly efficient, but a fraction of the electrical power is dissipated in the integrated circuit and the planar inductor. This thermal dissipation has a negative consequence on the OLED characteristics. Additionally the planar inductor represents a loop antenna that radiates electromagnetic energy. The radiated disturbance of the planar inductor must conform to the EMC standards. The COMSOL Multiphysics is used to investigate both the electromagnetic and thermal performance of the OLED module.

Keywords: thick film inductor, OLED, electromagnetic modelling, thermal modelling

1. Introduction

The electronics on flexible foils is an area of intensive research and development [1]-[4]. The electronics on flexible foils include the areas of wearable electronics, lightning devices and displays. Such electronics applications may require a power source embedded in the flexible foil and DC-DC converters are regularly used for this purpose because of their high efficiency [5].

The OLED module analysed in this paper is powered by a DC-DC converter consisting of an integrated circuit and a planar spiral inductor [6]. The integrated circuit and the planar inductor are embedded in the PET foil and form the backplane of the OLED module. The backplane is connected to the OLED tile via an adhesive layer. Figure 1 shows the general structure of an OLED module.

The backplane of the OLED module consists of the PET foil with aluminium metallization on both sides. The planar inductor etched in the PET foil aluminium is sandwiched between two Ferrite Polymer Composite (FPC) layers. These layers are used to shield the inductor from the OLED cathode. Figure 2 shows the described substrate structure.

The DC-DC converter of the OLED module places a number of requirements on the electrical characteristics of the inductor. The series inductance needs to be in a certain range for the converter to operate properly. The series resistance and the port capacitances need to be low enough to reduce the power dissipation. The resonant frequency needs to be significantly higher than the operating frequency of the converter f = 10 MHz.

An OLED module is a lightning device and it has to conform to the EMC standards. Such a standard is CISPR 15 [7] and it defines the radiated disturbance limit of the converter as the maximum electrical field at the distance of 10 m. The planar inductor was designed taking into account its electrical characteristics and EMC compliance [8].

The OLED is made of the organic material that is extremely sensitive to thermal influences [9]. The critical parameters that need to be fulfilled for normal operation of the OLED element is the operating temperature and the maximum temperature difference across the OLED element. Exceeding these requirements contributes to accelerated aging of the OLED element and its uneven illumination.

2. Governing equations

2.1 Electromagnetic theory

The modelled OLED module is analysed in the RF module in the frequency domain. The COMSOL Multiphysics software solves the differential equation (1) over the defined domains of the model. The equation is solved for the electrical field vector $\boldsymbol{E}$ at the frequency ω.

$$\nabla \times \mu_r^{-1}(\nabla \times \boldsymbol{E}) - k_0^2\left(\varepsilon_r - \frac{j\sigma}{\omega\varepsilon_0}\right)\boldsymbol{E} = \boldsymbol{0} \quad (1)$$

where k_0 is the wave number in free space and μ_r, ε_r and σ define the domain material electromagnetic properties: the relative

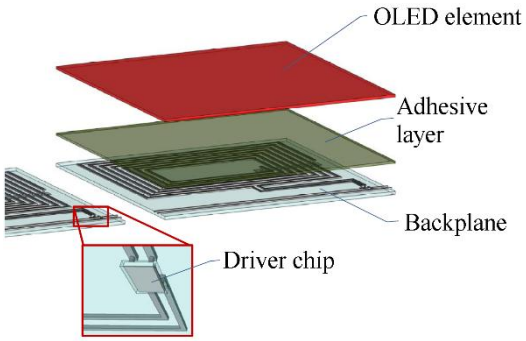

Figure 1. The general structure of the OLED module.

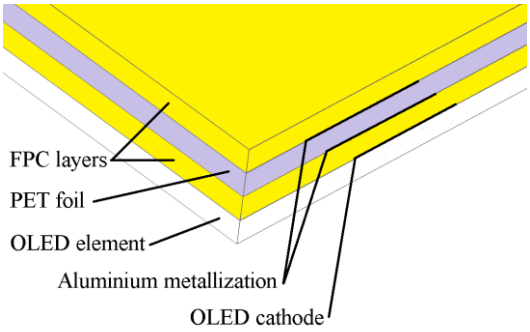

Figure 2. The substrate structure of the OLED module.

permeability, the relative permittivity and the conductivity.

2.2 Heat transfer theory

The OLED module model is analysed in the Heat Transfer module in the stationary state. The COMSOL Multiphysics software solves the differential equation (2) for the temperature *T*.

$$\rho C_p \boldsymbol{u} \cdot \nabla T = \nabla \cdot (k \nabla T) + Q \qquad (2)$$

where Q is the heat flux by conduction, $\boldsymbol{u}$ is the velocity vector and ρ, C_p and k define the domain material thermal properties: the density, the specific heat capacity at constant pressure and the thermal conductivity.

3. Methods

3.1 Use of COMSOL Multiphysics

The electromagnetic analysis of the OLED module is based on the RF Module (*emw*) of the COMSOL Multiphysics and the thermal analysis is based on the Heat Transfer in Solids Module (*ht*). The electromagnetic analysis is done in the frequency domain, while the thermal analysis is done in the stationary mode.

The geometry of the model is based on the OLED structure shown in Figure 1 and the resulting substrate structure shown in Figure 2. The layers are modelled in geometry as blocks while the metallization layers are modelled as the boundaries of the appropriate blocks. This allows the simulation of the very thin metallization layers (via the corresponding physics interfaces). The inductor metallization pattern is imported in to the geometry via a GDS file. The surrounding air is modelled in geometry by a two-layered sphere. The outer layer of the sphere is defined as the Infinite Element Domain and the inner layer is used for far-field calculations.

The surrounding air and the aluminium metallization properties are defined by the built-in materials, while the PET foil and the Ferrite Polymer Composite are defined by custom materials.

The RF Module is used in simulations to evaluate the electrical characteristics of the planar inductor and then to evaluate the far-field radiation and the heat dissipation due to the resistive losses. The planar inductor is a 2 port structure and it is defined by two Lumped Ports. The electrical characteristics are evaluated based on S-parameters. The RF Module is in this case used to make the port sweep and the Lumped Ports are set to Cable terminal type. When evaluating the far-field radiation and the inductor heating, the Lumped Ports are set to the Current Terminal port.

The far-field calculation is done by a Far-Field Domain defined in the inner layer of the sphere surrounding the OLED module model. The aluminium metallization is defined as the Transition Boundary Condition thus avoiding the meshing of very thin films.

The thermal modelling is based on the heating produced by the planar inductor and the DC-DC converter integrated circuit. The planar inductor is defined as a Boundary Heat Source and it is coupled with the RF Module physics via the *emw.Qsrh* variable. The integrated circuit is as well defined as a Boundary Heat Source over a 2x2 mm^2 boundary area. Its total boundary power is set to the approximated thermal dissipation of

the integrated circuit. The heat spreader is defined as a Highly Conductive Layer thus avoiding the meshing of very thin films similarly as in the RF Module. The heat spreader is defined in place of the OLED cathode.

The mesh of the complete geometry consists of three separate meshes. The OLED module itself and the core of the sphere containing the module are meshed with two separate Free Tetrahedral meshes. The inner and the outer layer of the sphere are meshed by a Swept mesh.

The model executes two separate studies. The first study sweeps the ports over a range of frequencies and thus produces the S-parameters of the planar inductor. The second study consists of two steps; the first step solves the Electromagnetic Waves physics in the frequency domain for a single frequency and the second step solves the Heat transfer physics in the stationary state. The second study sweeps the heat spreader thickness in a logarithmic manner.

The results in the context of the electrical characteristics are evaluated in a table based on the relations (3)-(8). The far-field radiation results are visualised via the Far Field component of the 3D Plot. The maximum far-field radiation is derived via the Surface Maximum function.

The results of the thermal analysis are based on the data selection made in the plane of the OLED element. The data selection is used to plot the temperature distribution and to determine the minimum and the maximum temperatures in the OLED material. The temperatures are determined by the corresponding Surface functions.

3.2 Electrical model

The two-port S-parameters of the planar inductor result from the RF Module simulations. To extract the relevant electrical characteristics of the inductor, these results require further processing. The S-parameters are used to model a simple π-network shown in Figure 3.

The network consists of three admittance elements: the port admittances Y_1 and Y_2, and the interport admittance Y_3. The inductor port capacitances C_1 and C_2 are extracted from the corresponding admittances Y_1 and Y_2, while the series inductance L_s and the series resistance R_s of the inductor are extracted from the interport admittance Y_3.

First, the S-parameters are converted to the Y-parameters which are related to the network

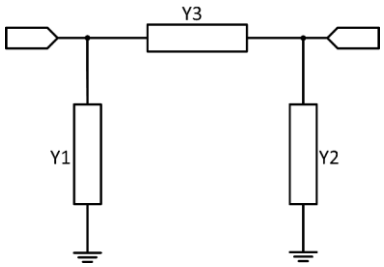

Figure 3. The π-network used to extract the electrical characteristics of the planar inductor.

admittances as shown in (3), (4) and (5). The electrical parameters of the inductor are then calculated from the network admittances based on the equations (6), (7) and (8). The parameters are extracted at the operating frequency of the DC-DC converter.

$$Y_1 = y_{11}+y_{12} \quad (3)$$

$$Y_2 = y_{22} + y_{12} \quad (4)$$

$$Y_3 = y_{12} = y_{21} \quad (5)$$

$$L_s = \frac{Im\{Y_3^{-1}\}}{\omega} \quad (6)$$

$$R_s = Re\{Y_3^{-1}\} \quad (7)$$

$$C_{1,2} = \frac{Im\{Y_{1,2}\}}{\omega} \quad (8)$$

4. Results

4.1 Electrical characteristics

The simulation results regarding the electrical characteristics of the planar inductor are presented in Figure 4 and Table 1.

Figure 4 shows the frequency characteristics of the inductor interport impedance and Table 1 shows the simulated values of the electrical parameters compared to the values required by the DC-DC converter.

The frequency characteristics show the behaviour of a typical inductor. The absolute impedance has a positive slope and a resonant frequency peak. The resonant frequency is at approximately 75 MHz and it is greater than the

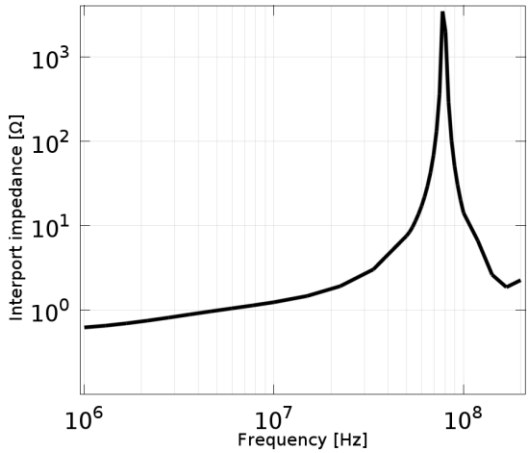

Figure 4. The interport impedance of the planar inductor.

Table 1. The results of the electrical characteristics analysis.

Electrical parameter	Simulated value	Required value
Series inductance L_S	1.42 µH	1 – 3 µH
Series resistance R_S	2.36 Ω	< 2 Ω
Port 1 capacitance C_1	0.327 pF	< 50 pF
Port 2 capacitance C_2	0.350 pF	< 50 pF
Resonant frequency f_r	~ 75 MHz	> 50 MHz

minimum 50 MHz frequency required by the DC-DC converter.

The electrical parameter values extracted from the simulation results based on the π-network model show that the parameters of the inductor do not completely conform to the requirements of the DC-DC converter.

4.2 Far-field radiation

The far-field radiation results are presented in Figure 5 and Table 3.

Figure 5 shows the far-field pattern in a 3D plot. The radiation pattern of the planar inductor is of toroidal shape which is expected for a loop antenna.

The maximum magnitude of the far-field radiation is compared to the required CISPR 15 limit in Table 3 and it shows that the far-field

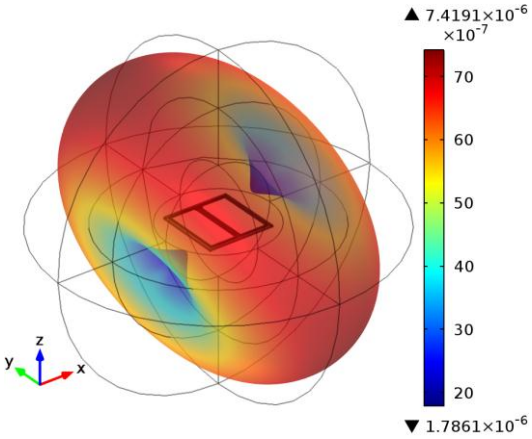

Figure 5. The 3D far-field radiation diagram.

Table 3. The results of the far-field radiation analysis.

Method / requirement	Max. electrical field* [dBµV/m]
Simulation	-2.59
CISPR 15 limit	< 30

* for distance r = 10 m

radiation of the planar inductor conforms to the EMC standard CISPR 15. It should be noted that the values in Table 3 are scaled to the distance of 10 m away from the OLED module.

4.3 Thermal performance

Figures 6, 7 and 8, and the Table 2 present the thermal performance of the OLED module.

Figure 6 shows the temperature distribution of the OLED element without the heat spreader. It shows a large gradient of the temperature across the OLED element and it is visible that the integrated circuit is the main heat source causing this temperature difference.

Table 2 compares the maximum OLED temperature and the maximum OLED

Table 2. The thermal performance analysis results of the OLED module without the heat spreader.

Thermal parameter	Simulated value	Required value
Maximum OLED temperature [°C]	67.6	< 70
Maximum OLED temperature difference [°C]	39.2	< 2

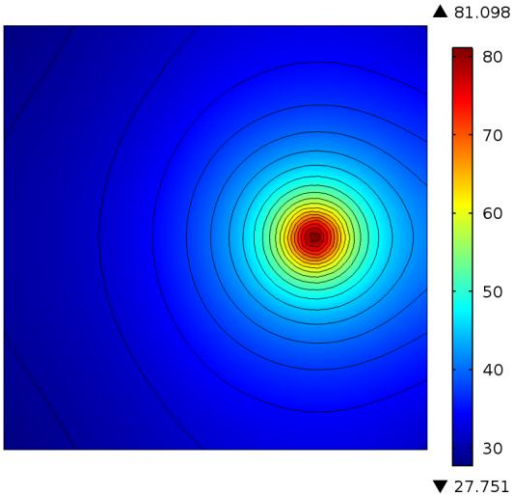

Figure 6. The thermal profile of the OLED tile without the heat spreader.

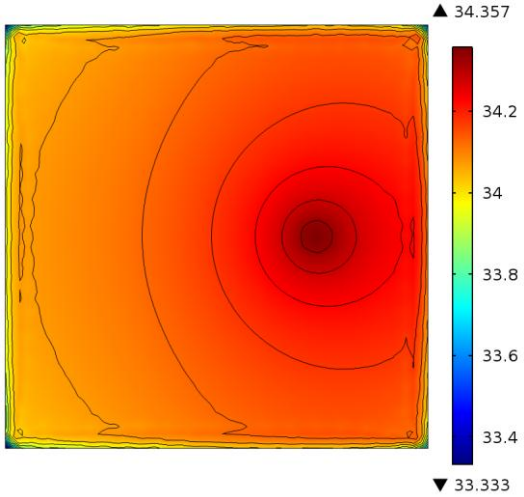

Figure 7. The thermal profile of the OLED tile with the heat spreader.

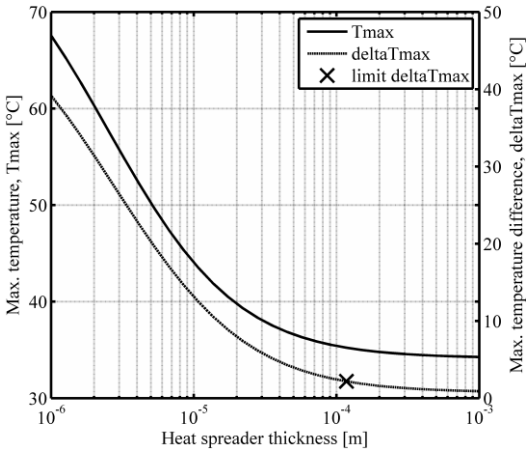

Figure 8. The maximum temperature and maximum temperature difference on the OLED tile w.r.t. the heat spreader thickness.

temperature difference with its required values for the case of the OLED module without the heat spreader. The maximum OLED temperature is just below the required value while the maximum OLED temperature difference is by an order of magnitude greater than the required value. This temperature difference is reduced by applying a heat spreader between the OLED element and its backplane.

Figure 8 shows the dependence of the OLED element maximum temperature and the temperature difference w.r.t. to the heat spreader thickness. The figure shows that by increasing the heat spreader thickness the maximum temperature and the maximum temperature difference decrease in a nonlinear fashion. The maximum OLED temperature conforms to the requirements over the whole range of the heat spreader thicknesses while the maximum OLED temperature difference conforms to the requirements for the heat spreader thicknesses greater than 100 µm.

Figure 7 shows that the application of the heat spreader greatly improves the thermal performance of the OLED module. The temperature distribution of the OLED element is smoother and conforms to the requirements set by the OLED material.

5. Discussion

The electrical characteristics of the planar inductor conform to the converter requirements with the exception of the series resistance. The series inductance is within the required range and the series resistance is higher than the required value. This will somewhat degrade the efficiency of the power conversion. The port capacitances are by orders of magnitude lower than the required value and this will have a positive effect on the converter efficiency. The resonant frequency of the inductor is high enough not to interfere with the operation of the converter. In the next inductor design iteration the inductor resistance will be reduced to the required value.

The far-field radiation of the inductor conforms to the requirements of the CISPR 15 standard. The radiation pattern is shaped as a tilted torus. This is similar to the radiation pattern of a loop antenna and the pattern tilt is probably caused by the port placement in the model.

The thermal analysis of the OLED module shows that the application of a heat spreader is necessary. The heat spreader lowers the operating temperature of the OLED element and brings its maximum temperature difference below the required value. This ensures an even illumination of the OLED element and reduces its aging.

6. Conclusions

An OLED module is analysed in the context of its electrical, electromagnetic and thermal characteristics. It is found that the electrical properties of the inductor partially meet the DC-DC converter requirements and that its radiated disturbance levels are lower than the required EMC limits. The thermal properties of the OLED module are improved by adding a heat spreader layer. The optimal thickness of the heat spreader is found to keep the maximum temperature difference across the OLED element within the required range.

7. References

1. I. Manunza, A. Sulis, A. Bonfiglio, "Organic semiconductor field effect transistors for unconventional applications: flexible sensors and wearable devices," *Proc. Int. Work. Wearable and Implantable Body Sensor Networks*, 2006, International Workshop on BSN 2006, pp. 3-5, April 2006.

2. C. D. Kim, J. S. Yoo, J. K. Lee, S. Y. Yoon, Y. I. Park, I. B. Kang; I. J. Chung, "Full color flexible displays on thin metal foil with reduced bending radius," *Proc. Flexible Electronics and Displays Conference and Exhibition*, 2009, pp. 1-4, Feb. 2009.

3. J.-S. Yoo, S.-H. Jung, Y.-C. Kim, S.-C. Byun, J.-M. Kim, N.-B. Choi, S.-Y. Yoon, C.-D. Kim, Y.-K. Hwang, I.-J. Chung, "Highly Flexible AM-OLED Display With Integrated Gate Driver Using Amorphous Silicon TFT on Ultrathin Metal Foil," *J. Display Technology*, vol. 6, no. 11, pp. 565-570, Nov. 2010.

4. E.C.W. de Jong, B.J.A. Ferreira, P. Bauer, "Toward the Next Level of PCB Usage in Power Electronic Converters," *IEEE Trans. Power Electronics*, vol. 23, no. 6, pp. 3151-3163, Nov. 2008.

5. Q. Li, M. Lim; J. Sun, A. Ball, Y. Ying, F. Lee, K.D.T., "Technology road map for high frequency integrated DC-DC converter," *IEEE Proc. Applied Power Electronics Conference and Exposition (APEC)*, 2010, pp. 533-539, Feb. 2010.

6. "Intelligent light management for OLED on foil applications (FP7-IMOLA) project", *http://www.imola-project.eu*, June 14, 2012.

7. *Limits and methods of measurement of radio disturbance characteristics of electrical lighting and similar equipment*, CISPR 15, 2009.

8. J. Kundrata, A. Baric, "Design of a planar inductor for DC-DC converter on flexible foil applications," *Proceedings of the 35th International Convention MIPRO 2012*, pp. 54-59, May 2012.

9. X. Zhou, J. He, L. S. Liao, M. Lu, X. M. Ding, X. Y. Hou, X. M. Zhang, X. Q. He, and S. T. Lee, "Real-Time Observation of Temperature Rise and Thermal Breakdown Processes in Organic LEDs Using an IR Imaging and Analysis System", *Advanced Materials*, vol. 12, pp. 265, 2000.

8. Acknowledgements

This work was supported by the European Commission under the Seventh Framework Programme (FP7) through project IMOLA „Intelligent light management for OLED on foil applications“(Grant Agreement No. 288377).